2026 IEEE International Conference on Robotics and Automation (ICRA 2026)
June 1-5, 2026. Vienna, Austria

On Robust Coordinated Compliant Control Design for Space Manipulators under Flexible and Uncertain Dynamics*

Kostas Nanos[1], and Evangelos Papadopoulos[2], *Life Fellow, IEEE*

***Abstract*— This paper presents a coordinated compliant control strategy for space manipulator systems to enable safe and robust target capture during on-orbit servicing and assembly missions. The proposed controller operates in two distinct phases: free-space motion and contact interaction. In the free-space phase, end-effector accurate trajectory tracking is required, while in the contact phase, the control objective shifts to force regulation, maintaining contact forces within safe bounds and ensuring stable interaction durations to enhance operational safety. A key feature of the developed method is its ability to provide a smooth and continuous transition between free-space and contact phases without requiring controller switching. Furthermore, the controller preserves the attitude stability of the chaser spacecraft during manipulation, mitigating mission-critical risks such as communication loss or solar panel misalignment. The approach explicitly incorporates the coupled rigid-body dynamics of the SMS and demonstrates robustness to various real-world disturbances. Simulation results validate the effectiveness of the proposed controller. Future work includes experiments, using the planar Space Robotics Emulator of our lab at the National Technical University of Athens to assess real-world readiness.**

I. Introduction

Robotic technologies for in-orbit missions must overcome numerous challenges due to the difficulties of the space environment, [1], [2]. During proximity rendezvous and docking missions, a Space Manipulator System (SMS) or chaser, needs to capture a cooperative or non-cooperative target, see Fig. 1. However, the impact between the chaser's end-effector (EE) and the target may lead to various adverse effects, such as contact loss and the development of large contact forces leading to manipulator damage and resulting capture mission failure.

To address capture impacts in space manipulation, several impedance and adaptive control methods have been proposed. Simplified impedance control with a prismatic joint can shape end-effector compliance [3] but is limited to non-standard manipulator designs. Prescribed Performance Control (PPC) combined with adaptive Radial Basis Function Neural Networks (RBFNN), enables accurate force/pose regulation [4]; Nonetheless, their stability can be sensitive to tuning of the learning dynamics, and robustness under realistic space conditions remains unverified. Adaptive optimal control methods for de-tumbling non-cooperative targets using repeated multipoint contact have also been explored [5], though solving equality-constrained problems in real time poses significant computational demands for onboard systems.

To increase the contact time between the EE and the target, the combined impedance and PD control has been proposed, [6]. However, this method only extends the contact time; it does not prevent contact loss.

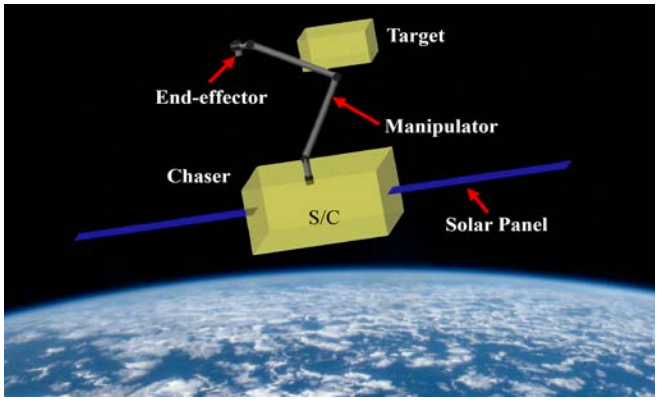

Fig. 1. A space manipulator system (chaser) capturing a space target.

To avoid contact loss, a collision control method, named Resistance Control (RC), has been proposed [7]. Although this method improves contact performance compared to previous approaches, it does not regulate the maximum contact force on the chaser during impact. Therefore, this method does not eliminate the risk of damage to both the chaser and the target.

To address this issue, an impedance-based sliding mode controller was proposed in [8], demonstrating regulation of the maximum contact force in simulation, though without preventing contact loss. Subsequently, the Reaction Control (RC) method in [7] was enhanced to Compliance Resistance Control (CRC) [9] to reduce contact loss and peak forces. However, CRC cannot fully suppress force overshoots that may endanger the chaser and the target.

Preventing force overshoots while avoiding contact loss remains a challenging issue. To tackle these and reduce mission risks, a *Coordinated Compliant Control* (CCC) law is developed enabling smooth free-to-contact phase transitions without switching, regulating contact forces and keeping spacecraft (S/C) attitude. This controller accounts for

* This research work was supported by the project "Applied Research for Autonomous Robotic Systems" (MIS5200632) which is implemented within the framework of the National Recovery and Resilience Plan (NNRP) "Greece 2.0" (Measure: 16618- Basic and Applied Research) and is funded by the European Union-NextGenerationEU.
[1]Department of Electrical and Electronic Engineering Educators, School of Pedagogical and Technological Education, Athens, Greece, e-mail: knanos@aspete.gr.
[2]Robotics Institute, Athena Research Center, Marousi, Greece, and School of Mechanical Engineering, National Technical University of Athens, Greece, egpapado@central.ntua.gr, phone: +30-210-772-1440.

coupled rigid-body dynamics and is robust to disturbances such as solar panel oscillations and sensor noise.

II. System Rigid Body Dynamics

In the context of SMS control, the system's rigid body dynamics play a crucial role in ensuring stable operation. In this section, the system equations of motion are written in a form suitable for the design of the developed model-based Coordinated Compliant Control law.

During capture, the EE must be driven properly to the contact point while simultaneously the S/C orientation must be controlled to a desired one using only the S/C Reaction Wheels (RWs) and manipulator joint motors. In this case, the system's controllable vector is given by,

$$\mathbf{v}_{cont} = \begin{bmatrix} \boldsymbol{\omega}_b^T & \mathbf{v}_e^T & \boldsymbol{\omega}_e^T \end{bmatrix}^T \tag{1}$$

where $\boldsymbol{\omega}_b$ is the S/C angular velocity and $\mathbf{v}_e$, $\boldsymbol{\omega}_e$ are the EE linear and angular velocities, respectively.

The applied actuation vector is,

$$\mathbf{Q}_c = \begin{bmatrix} \boldsymbol{\tau}_{rw}^T & \boldsymbol{\tau}^T \end{bmatrix}^T \tag{2}$$

where $\boldsymbol{\tau}$ and $\boldsymbol{\tau}_{rw}$ are the column vectors of the manipulator joints and the reaction wheels torques, respectively.

To introduce the gyroscopic effects due to the rotation of the S/C RWs, the derivation of the equations of motion also considers RWs dynamics.

Next, the equations of motion in *Joint – Space* are briefly presented (Section II.1). Then, using an appropriate Jacobian matrix, the equations are converted to the *Cartesian space* (Section II.2). Finally, the desired *reduced* equations of motion in Cartesian space, with generalized coordinates $\mathbf{v}_{cont}$ and generalized forces $\mathbf{Q}_c$, as defined by (1) and (2), respectively, are derived (Section II.3).

II.1. Joint space equations of motion

The joint space dynamics are described by,

$$\mathbf{M}_q \dot{\mathbf{v}}_q + \mathbf{c}_q = \mathbf{Q}_{act} + \mathbf{Q}_{ext} \tag{3}$$

where $\mathbf{M}_q$ and $\mathbf{c}_q$ are the system inertia matrix and the nonlinear velocity-dependent vector, respectively, and

$$\mathbf{v}_q = \begin{bmatrix} \mathbf{v}_b^T & \boldsymbol{\omega}_b^T & \dot{\mathbf{q}}_{rw}^T & \dot{\mathbf{q}}^T \end{bmatrix}^T \tag{4}$$

where $\mathbf{v}_b$, is the S/C linear velocity, $\mathbf{q}$ denotes the manipulator joint angles, $\mathbf{q}_{rw}$ denotes the RW angles and $\dot{(\cdot)}$ denotes the time derivative of $(\cdot)$.

The generalized forces $\mathbf{Q}_{act}$, are due to actuation forces and are given by,

$$\mathbf{Q}_{act} = \mathbf{J}_c^T \begin{bmatrix} \mathbf{R}_b \, {}^b\mathbf{f}_b \\ \mathbf{R}_b \, {}^b\mathbf{n}_b \\ \boldsymbol{\tau}_{rw} \\ \boldsymbol{\tau} \end{bmatrix} \tag{5}$$

where ${}^b\mathbf{f}_b$, ${}^b\mathbf{n}_b$ denote the external forces and moments, respectively, acting on the S/C due to thruster forces and expressed in the S/C frame, $\mathbf{R}_b$ is the rotation matrix between the S/C frame and the inertial frame and $\mathbf{J}_c$ is an appropriate Jacobian matrix.

The generalized forces $\mathbf{Q}_{ext}$, correspond to the external forces caused by contact forces, and are given by,

$$\mathbf{Q}_{ext} = \mathbf{J}_e^T \begin{bmatrix} \mathbf{f}_e^T & \mathbf{n}_e^T \end{bmatrix}^T = \mathbf{J}_e^T \boldsymbol{F}_{ext} \tag{6}$$

where $\mathbf{f}_e$, $\mathbf{n}_e$ denote the external (contact) forces and moments, respectively, applied on the EE and expressed in the inertial frame. The Jacobian matrix $\mathbf{J}_e$ is defined by

$$\begin{bmatrix} \mathbf{v}_e^T & \boldsymbol{\omega}_e^T \end{bmatrix}^T = \mathbf{J}_e \, \mathbf{v}_q \tag{7}$$

The EE linear and angular velocities are given, respectively, by

$$\mathbf{v}_e = \mathbf{v}_b + \mathbf{J}_{v\omega} \, \boldsymbol{\omega}_b + \mathbf{J}_{vq} \, \dot{\mathbf{q}} \tag{8}$$

$$\boldsymbol{\omega}_e = \boldsymbol{\omega}_b + \mathbf{J}_{\omega q} \, \dot{\mathbf{q}} \tag{9}$$

where $\mathbf{J}_{v\omega}$, $\mathbf{J}_{vq}$ and $\mathbf{J}_{\omega q}$ are Jacobian-type matrices.

Eqs. (8) - (9) can be written in matrix form as:

$$\begin{bmatrix} \mathbf{v}_e \\ \boldsymbol{\omega}_e \end{bmatrix} = \begin{bmatrix} \mathbf{I}_3 & \mathbf{J}_{v\omega} & \mathbf{0}_{3xN_{rw}} & \mathbf{J}_{vq} \\ \mathbf{0}_{3\times3} & \mathbf{I}_3 & \mathbf{0}_{3xN_{rw}} & \mathbf{J}_{\omega q} \end{bmatrix} \mathbf{v}_q \tag{10}$$

where $\mathbf{0}_{n\times m}$ is the $n\times m$ zero matrix, $\mathbf{I}_n$ is the $n\times n$ identity matrix and N_{rw} is the number of RWs.

Thus, (7) and (10) yield,

$$\mathbf{J}_e = \begin{bmatrix} \mathbf{I}_3 & \mathbf{J}_{v\omega} & \mathbf{0}_{3xN_{rw}} & \mathbf{J}_{vq} \\ \mathbf{0}_{3\times3} & \mathbf{I}_3 & \mathbf{0}_{3xN_{rw}} & \mathbf{J}_{\omega q} \end{bmatrix} \tag{11}$$

II.2. Cartesian space equations of motion

The generalized velocity column vector $\mathbf{v}_x$ is defined as,

$$\mathbf{v}_x = \begin{bmatrix} \mathbf{v}_b^T & \boldsymbol{\omega}_b^T & \dot{\mathbf{q}}_{rw}^T & \mathbf{v}_e^T & \boldsymbol{\omega}_e^T \end{bmatrix}^T \tag{12}$$

and is related to the generalized velocity $\mathbf{v}_q$ via a Jacobian-type matrix $\mathbf{J}_x$,

$$\mathbf{v}_x = \mathbf{J}_x \, \mathbf{v}_q \tag{13}$$

where,

$$\mathbf{J}_x = \begin{bmatrix} \mathbf{I}_3 & \mathbf{0}_{3x3} & \mathbf{0}_{3xN_{rw}} & \mathbf{0}_{3xN_m} \\ \mathbf{0}_{3x3} & \mathbf{I}_3 & \mathbf{0}_{3xN_{rw}} & \mathbf{0}_{3xN_m} \\ \mathbf{0}_{N_{rw}x3} & \mathbf{0}_{N_{rw}x3} & \mathbf{I}_{N_{rw}} & \mathbf{0}_{N_{rw}xN_m} \\ \mathbf{I}_3 & \mathbf{J}_{v\omega} & \mathbf{0}_{3xN_{rw}} & \mathbf{J}_{vq} \\ \mathbf{0}_{3x3} & \mathbf{I}_3 & \mathbf{0}_{3xN_{rw}} & \mathbf{J}_{\omega q} \end{bmatrix} \tag{14}$$

where N_m is the number of manipulator joints.

Considering (13), the joint space dynamics, given by (3), are transformed to the following Cartesian space dynamics,

$$\mathbf{M}_x \dot{\mathbf{v}}_x + \mathbf{c}_x = \mathbf{J}_{c,x}^T \mathbf{Q}_{act} + \mathbf{J}_{e,x}^T \boldsymbol{F}_{ext} \tag{15}$$

where for *non-redundant* manipulators (i.e., $N_m = 6$),

$$\mathbf{M}_x = \mathbf{J}_x^{-T} \mathbf{M}_q \mathbf{J}_x^{-1} \tag{16}$$

$$\mathbf{c}_x = \mathbf{J}_x^{-T} \left(\mathbf{c}_q - \mathbf{M}_q \mathbf{J}_x^{-1} \dot{\mathbf{J}}_x \mathbf{v}_q \right) \tag{17}$$

$$\mathbf{J}_{c,x}^T = \mathbf{J}_x^{-T} \mathbf{J}_c^T \tag{18}$$

$$\mathbf{J}_{e,x}^T = \mathbf{J}_x^{-T} \mathbf{J}_e^T \tag{19}$$

Note that, for *redundant* manipulators (i.e., $N_m > 6$), the matrix $\mathbf{J}_x$ is not a square matrix, and thus not invertible. In this case, it can be shown that,

$$\mathbf{M}_x = (\mathbf{J}_x \mathbf{M}_q^{-1} \mathbf{J}_x^T)^{-1} \tag{20}$$

$$\mathbf{c}_x = (\mathbf{J}_x \mathbf{M}_q^{-1} \mathbf{J}_x^T)^{-1} (\mathbf{J}_x \mathbf{M}_q^{-1} \mathbf{c}_q - \dot{\mathbf{J}}_x \mathbf{v}_q) \tag{21}$$

$$\mathbf{J}_{c,x}^T = (\mathbf{J}_x \mathbf{J}_x^T)^{-1} \mathbf{J}_x \mathbf{J}_c^T \tag{22}$$

$$\mathbf{J}_{e,x}^T = (\mathbf{J}_x \mathbf{M}_q^{-1} \mathbf{J}_x^T)^{-1} \mathbf{J}_x \mathbf{M}_q^{-1} \mathbf{J}_e^T \tag{23}$$

II.3. Reduced equations of motion

As mentioned above, during capture, the chaser S/C can use its RWs for attitude control (here a standard configuration of 4 RWs is considered), but the chaser thrusters are turned-off for safety, due to its proximity to the target. Thus, $\boldsymbol{\tau}$ and $\boldsymbol{\tau}_{rw}$ are the control inputs and in (5) ${}^b\mathbf{f}_b = {}^b\mathbf{n}_b = \mathbf{0}_{3\times1}$. Moreover, since contact is expected at the end effector, in (6) $\mathbf{f}_e \neq \mathbf{0}_{3\times1}$ and $\mathbf{n}_e \neq \mathbf{0}_{3\times1}$. With these control inputs, not all velocities can be controlled. The controllable vector is given by (1) while the uncontrollable vector is,

$$\mathbf{v}_{uncont} = \begin{bmatrix} \mathbf{v}_b^T & \dot{\mathbf{q}}_{rw}^T \end{bmatrix}^T \tag{24}$$

Eq. (15) can be rewritten in the following form,

$$\underbrace{\begin{bmatrix} \hat{\mathbf{M}}_{11} & \hat{\mathbf{M}}_{12} & \mathbf{0}_{3\times3} & \hat{\mathbf{M}}_{14} & \hat{\mathbf{M}}_{15} \\ \hat{\mathbf{M}}_{21} & \hat{\mathbf{M}}_{22} & \hat{\mathbf{M}}_{23} & \hat{\mathbf{M}}_{24} & \hat{\mathbf{M}}_{25} \\ \mathbf{0}_{3\times3} & \hat{\mathbf{M}}_{32} & \hat{\mathbf{M}}_{33} & \hat{\mathbf{M}}_{34} & \hat{\mathbf{M}}_{35} \\ \hat{\mathbf{M}}_{41} & \hat{\mathbf{M}}_{42} & \hat{\mathbf{M}}_{43} & \hat{\mathbf{M}}_{44} & \hat{\mathbf{M}}_{45} \\ \hat{\mathbf{M}}_{51} & \hat{\mathbf{M}}_{52} & \hat{\mathbf{M}}_{53} & \hat{\mathbf{M}}_{54} & \hat{\mathbf{M}}_{55} \end{bmatrix}}_{\mathbf{M}_x} \begin{bmatrix} \dot{\mathbf{v}}_b \\ \dot{\boldsymbol{\omega}}_b \\ \ddot{\mathbf{q}}_{rw} \\ \dot{\mathbf{v}}_e \\ \dot{\boldsymbol{\omega}}_e \end{bmatrix} + \underbrace{\begin{bmatrix} \mathbf{c}_{vb} \\ \mathbf{c}_{\omega b} \\ \mathbf{c}_{rw} \\ \mathbf{c}_{ve} \\ \mathbf{c}_{\omega e} \end{bmatrix}}_{\mathbf{c}_x} =$$

$$= \underbrace{\begin{bmatrix} \hat{\mathbf{J}}_{c11}^T & \hat{\mathbf{J}}_{c21}^T & \hat{\mathbf{J}}_{c31}^T & \hat{\mathbf{J}}_{c41}^T \\ \hat{\mathbf{J}}_{c12}^T & \hat{\mathbf{J}}_{c22}^T & \hat{\mathbf{J}}_{c32}^T & \hat{\mathbf{J}}_{c42}^T \\ \hat{\mathbf{J}}_{c13}^T & \hat{\mathbf{J}}_{c23}^T & \hat{\mathbf{J}}_{c33}^T & \hat{\mathbf{J}}_{c43}^T \\ \hat{\mathbf{J}}_{c14}^T & \hat{\mathbf{J}}_{c24}^T & \hat{\mathbf{J}}_{c34}^T & \hat{\mathbf{J}}_{c44}^T \\ \hat{\mathbf{J}}_{c15}^T & \hat{\mathbf{J}}_{c25}^T & \hat{\mathbf{J}}_{c35}^T & \hat{\mathbf{J}}_{c45}^T \end{bmatrix}}_{\mathbf{J}_{c,x}^T} \begin{bmatrix} \mathbf{0}_{3\times1} \\ \mathbf{0}_{3\times1} \\ \boldsymbol{\tau}_{rw} \\ \boldsymbol{\tau} \end{bmatrix} + \underbrace{\begin{bmatrix} \hat{\mathbf{J}}_{e11}^T & \hat{\mathbf{J}}_{e21}^T \\ \hat{\mathbf{J}}_{e12}^T & \hat{\mathbf{J}}_{e22}^T \\ \hat{\mathbf{J}}_{e13}^T & \hat{\mathbf{J}}_{e23}^T \\ \hat{\mathbf{J}}_{e14}^T & \hat{\mathbf{J}}_{e24}^T \\ \hat{\mathbf{J}}_{e15}^T & \hat{\mathbf{J}}_{e25}^T \end{bmatrix}}_{\mathbf{J}_{e,x}^T} \begin{bmatrix} \mathbf{f}_e \\ \mathbf{n}_e \end{bmatrix} \tag{25}$$

where it is also considered that ${}^b\mathbf{f}_b = {}^b\mathbf{n}_b = \mathbf{0}_{3\times1}$ and $\hat{\mathbf{M}}_{ij}$, $\hat{\mathbf{J}}_{cji}^T$, $\hat{\mathbf{J}}_{eij}^T$ are matrix elements of the matrices $\mathbf{M}_x$, $\mathbf{J}_{c,x}^T$, $\mathbf{J}_{e,x}^T$ respectively.

It can be shown that eliminating the uncontrollable variables $\mathbf{v}_b$ and $\dot{\mathbf{q}}_{rw}$ from Eq. (25), the *reduced* dynamics have the form:

$$\bar{\mathbf{M}}\dot{\mathbf{v}}_{cont} + \bar{\mathbf{c}} = \bar{\mathbf{J}}_c{}^T \mathbf{Q}_c + \bar{\mathbf{J}}_e{}^T \boldsymbol{F}_{ext} \tag{26}$$

where the column vectors $\mathbf{v}_{cont}$ and $\mathbf{Q}_c$ are defined by (1) and (2), respectively, and the matrix $(\bar{\bullet})$ corresponds to the matrix $(\bullet)$ of the reduced system, given by,

$$\bar{\mathbf{M}} = \begin{bmatrix} \bar{\mathbf{M}}_{11} & \bar{\mathbf{M}}_{12} & \bar{\mathbf{M}}_{13} \\ \bar{\mathbf{M}}_{21} & \bar{\mathbf{M}}_{22} & \bar{\mathbf{M}}_{23} \\ \bar{\mathbf{M}}_{31} & \bar{\mathbf{M}}_{32} & \bar{\mathbf{M}}_{33} \end{bmatrix}, \bar{\mathbf{J}}_c^T = \begin{bmatrix} \bar{\mathbf{J}}_{c,11}^T & \bar{\mathbf{J}}_{c,12}^T \\ \bar{\mathbf{J}}_{c,21}^T & \bar{\mathbf{J}}_{c,22}^T \\ \bar{\mathbf{J}}_{c,31}^T & \bar{\mathbf{J}}_{c,32}^T \end{bmatrix}, \bar{\mathbf{J}}_E^T = \begin{bmatrix} \bar{\mathbf{J}}_{e,11}^T & \bar{\mathbf{J}}_{e,12}^T \\ \bar{\mathbf{J}}_{e,21}^T & \bar{\mathbf{J}}_{e,22}^T \\ \bar{\mathbf{J}}_{e,31}^T & \bar{\mathbf{J}}_{e,32}^T \end{bmatrix} \tag{27}$$

where the matrices $\bar{\mathbf{M}}_{ij}$, $\bar{\mathbf{J}}_{c,\mathrm{ij}}^T$ and $\bar{\mathbf{J}}_{e,\mathrm{ij}}^T$, which are functions of the matrices $\hat{\mathbf{M}}_{ij}, \hat{\mathbf{J}}_{cij}^T, \hat{\mathbf{J}}_{eij}^T$, with $i, j = 1,...,5$, are not given here due to space constraints, and

$$\bar{\mathbf{c}} = \begin{bmatrix} \mathbf{c}_{\omega b} - \hat{\mathbf{M}}_{21}\hat{\mathbf{M}}_{11}^{-1}\mathbf{c}_{vb} - \hat{\mathbf{M}}_{23}\hat{\mathbf{M}}_{33}^{-1}\mathbf{c}_{rw} \\ \mathbf{c}_{ve} - \hat{\mathbf{M}}_{41}\hat{\mathbf{M}}_{11}^{-1}\mathbf{c}_{vb} - \hat{\mathbf{M}}_{43}\hat{\mathbf{M}}_{33}^{-1}\mathbf{c}_{rw} \\ \mathbf{c}_{\omega e} - \hat{\mathbf{M}}_{51}\hat{\mathbf{M}}_{11}^{-1}\mathbf{c}_{vb} - \hat{\mathbf{M}}_{53}\hat{\mathbf{M}}_{33}^{-1}\mathbf{c}_{rw} \end{bmatrix} \tag{28}$$

The uncontrollable variables $\mathbf{v}_b$, $\dot{\mathbf{q}}_{rw}$ are described by

$$\begin{aligned} \dot{\mathbf{v}}_b = {} & \hat{\mathbf{M}}_{11}^{-1}\left(-\mathbf{c}_{vb} - \hat{\mathbf{M}}_{12}\dot{\boldsymbol{\omega}}_b - \hat{\mathbf{M}}_{14}\dot{\mathbf{v}}_e - \hat{\mathbf{M}}_{15}\dot{\boldsymbol{\omega}}_e\right) \\ & + \hat{\mathbf{M}}_{11}^{-1}\left(\hat{\mathbf{J}}_{c31}^T\boldsymbol{\tau}_{rw} + \hat{\mathbf{J}}_{c41}^T\boldsymbol{\tau} + \hat{\mathbf{J}}_{c11}^T\mathbf{f}_e + \hat{\mathbf{J}}_{c21}^T\mathbf{n}_e\right) \end{aligned} \tag{29}$$

$$\begin{aligned} \ddot{\mathbf{q}}_{rw} = {} & \hat{\mathbf{M}}_{33}^{-1}\left(-\mathbf{c}_{rw} - \hat{\mathbf{M}}_{32}\dot{\boldsymbol{\omega}}_b - \hat{\mathbf{M}}_{34}\dot{\mathbf{v}}_e - \hat{\mathbf{M}}_{35}\dot{\boldsymbol{\omega}}_e\right) \\ & + \hat{\mathbf{M}}_{33}^{-1}\left(\hat{\mathbf{J}}_{c33}^T\boldsymbol{\tau}_{rw} + \hat{\mathbf{J}}_{c43}^T\boldsymbol{\tau} + \hat{\mathbf{J}}_{c13}^T\mathbf{f}_e + \hat{\mathbf{J}}_{c23}^T\mathbf{n}_e\right) \end{aligned} \tag{30}$$

Eq. (26) will be employed in the design of the proposed control law presented in the next section.

III. Controller Design

During a capture task, the motion can be divided in two phases: (i) the *free-space phase*, and (ii) the *contact phase*, [10] - [11]. The main aim of the developed control law, called Coordinated Compliant Control (CCC), is to cause the desired behavior of the EE in both phases without requiring controller switching while simultaneously controlling the S/C orientation to a desired one. Applying the CCC, not only results in a desired contact time but also sets a desired and predefined upper limit to the contact force. This leads to safe target capture avoiding contact loss and large contact forces which may result in manipulator and/ or target damage.

To describe the chaser S/C and EE orientation, the Euler angles approach is adopted. Euler Parameters can be used, also. Using Euler angles, the new controllable vector is,

$$\bar{\mathbf{v}}_{cont} = \begin{bmatrix} \dot{\boldsymbol{\theta}}_b^T & \mathbf{v}_e^T & \dot{\boldsymbol{\theta}}_e^T \end{bmatrix}^T \tag{31}$$

where $\boldsymbol{\theta}_b$ and $\boldsymbol{\theta}_e$ are the chaser S/C and chaser EE Euler angles column vectors, respectively.

The controllable vectors $\bar{\mathbf{v}}_{cont}$ and $\mathbf{v}_{cont}$, defined by (1), are related by,

$$\mathbf{v}_{cont} = \mathbf{E}^*(\boldsymbol{\theta}_b, \boldsymbol{\theta}_e)\bar{\mathbf{v}}_{cont} \tag{32}$$

where

$$\mathbf{E}^*(\boldsymbol{\theta}_b, \boldsymbol{\theta}_e) = \begin{bmatrix} \mathbf{E}(\boldsymbol{\theta}_b) & \mathbf{0}_{3\times3} & \mathbf{0}_{3\times3} \\ \mathbf{0}_{3\times3} & \mathbf{I}_3 & \mathbf{0}_{3\times3} \\ \mathbf{0}_{3\times3} & \mathbf{0}_{3\times3} & \mathbf{E}(\boldsymbol{\theta}_e) \end{bmatrix} \tag{33}$$

where $\mathbf{E}(\boldsymbol{\theta}_b)$ and $\mathbf{E}(\boldsymbol{\theta}_e)$ are 3x3 appropriate matrices.

Using (32), it can be shown that (26) takes the form,

$$\bar{\mathbf{M}}^*\dot{\bar{\mathbf{v}}}_{cont} + \bar{\mathbf{c}}^* = \bar{\mathbf{J}}_c{}^{T*}\mathbf{Q}_c + \bar{\mathbf{J}}_e{}^{T*}\boldsymbol{F}_{ext} \tag{34}$$

where

$$\bar{\mathbf{M}}^* = \mathbf{E}^{*T}(\boldsymbol{\theta}_b, \boldsymbol{\theta}_e)\bar{\mathbf{M}}\,\mathbf{E}^*(\boldsymbol{\theta}_b, \boldsymbol{\theta}_e) \tag{35}$$

$$\bar{\mathbf{c}}^* = \mathbf{E}^{*T}(\boldsymbol{\theta}_b, \boldsymbol{\theta}_e)\bar{\mathbf{c}} + \mathbf{E}^{*T}(\boldsymbol{\theta}_b, \boldsymbol{\theta}_e)\,\dot{\mathbf{E}}^{*T}(\boldsymbol{\theta}_b, \boldsymbol{\theta}_e, \dot{\boldsymbol{\theta}}_b, \dot{\boldsymbol{\theta}}_e)\,\bar{\mathbf{v}}_{cont} \tag{36}$$

$$\bar{\mathbf{J}}_c{}^{T*} = \mathbf{E}^{*T}(\boldsymbol{\theta}_b, \boldsymbol{\theta}_e)\bar{\mathbf{J}}_c{}^T \quad , \quad \bar{\mathbf{J}}_e{}^{T*} = \mathbf{E}^{*T}(\boldsymbol{\theta}_b, \boldsymbol{\theta}_e)\bar{\mathbf{J}}_e{}^T \tag{37}$$

The developed Coordinated Compliant Control law is,

$$\mathbf{Q}_{contr} = \bar{\mathbf{M}}^{*}\mathbf{u} + \bar{\mathbf{c}}^{*} - \bar{\mathbf{J}}_{e}^{T^{*}}\boldsymbol{F}_{ext} \tag{38}$$

where

$$\mathbf{Q}_{contr} = \bar{\mathbf{J}}_{c}^{T^{*}}\mathbf{Q}_{c} \tag{39}$$

$$\mathbf{u} = \begin{bmatrix} \mathbf{u}_b \\ \mathbf{u}_e \end{bmatrix} = \begin{bmatrix} \ddot{\boldsymbol{\theta}}_{b,d} - \mathbf{K}_{d,b}\dot{\mathbf{e}}_b - \mathbf{K}_{p,b}\mathbf{e}_b \\ \ddot{\mathbf{x}}_{e,d} + \mathbf{M}_{d,e}^{-1}\left(-\mathbf{K}_{d,\mathrm{e}}\dot{\mathbf{e}}_e - \mathbf{K}_{p,\mathrm{e}}\mathbf{e}_e - \boldsymbol{F}_{ext} + \boldsymbol{F}_{des}\right) \end{bmatrix} \tag{40}$$

where $(\bullet)_d$ denotes the desired value of $(\bullet)$ and

$$\mathbf{x}_e = \begin{bmatrix} \mathbf{r}_{\mathrm{e}}^{T} & \boldsymbol{\theta}_{\mathrm{e}}^{T} \end{bmatrix}^{T} \tag{41}$$

where $\mathbf{r}_{\mathrm{e}}$ is the EE position and $\boldsymbol{\theta}_{\mathrm{e}}$ its orientation.

The control law $\mathbf{u}_b$ corresponds to a PD control input for the S/C attitude with control gains $\mathbf{K}_{d,b}$ and $\mathbf{K}_{p,b}$ while the control law $\mathbf{u}_e$ corresponds to an impedance controller for the chaser EE, where $\mathbf{M}_{d,e}, \mathbf{K}_{d,\mathrm{e}}, \mathbf{K}_{p,\mathrm{e}}$ are its impedance gains, and $\boldsymbol{F}_{des}$ is a non-zero constant column vector setting the desired contact force.

The vectors $\mathbf{e}_b$ and $\mathbf{e}_e$ are the S/C attitude trajectory error and EE pose (i.e., position/ orientation) trajectory error, respectively, defined as,

$$\mathbf{e}_b = \boldsymbol{\theta}_b - \boldsymbol{\theta}_{b,d} \tag{42}$$

$$\mathbf{e}_e = \mathbf{x}_e - \mathbf{x}_{e,d} = [\mathbf{r}_e^{T} \quad \boldsymbol{\theta}_e^{T}]^{T} - [\mathbf{r}_{e,d}^{T} \quad \boldsymbol{\theta}_{e,d}^{T}]^{T} \tag{43}$$

Eq. (40) can be also written compactly as,

$$\mathbf{u} = \begin{bmatrix} \mathbf{u}_b^{T} & \mathbf{u}_e^{T} \end{bmatrix}^{T} = \ddot{\mathbf{z}}_d + \mathbf{M}_d^{-1}\left(-\mathbf{K}_d\,\dot{\mathbf{e}} - \mathbf{K}_p\,\mathbf{e} - \boldsymbol{F}_{ext}^{*} + \boldsymbol{F}_{des}^{*}\right) \tag{44}$$

where

$$\mathbf{e} = \begin{bmatrix} \mathbf{e}_b^{T} & \mathbf{e}_e^{T} \end{bmatrix}^{T} = \mathbf{z} - \mathbf{z}_d \tag{45}$$

$$\mathbf{z} = \begin{bmatrix} \boldsymbol{\theta}_b^{T} & \mathbf{x}_e^{T} \end{bmatrix}^{T} \tag{46}$$

$$\boldsymbol{F}_{ext}^{*} = \begin{bmatrix} \mathbf{0}_{3\times1}^{T} & \boldsymbol{F}_{ext}^{T} \end{bmatrix}^{T} \tag{47}$$

and

$$\mathbf{M}_d = \begin{bmatrix} \mathbf{I}_3 & \mathbf{0}_{3\times6} \\ \mathbf{0}_{6\times3} & \mathbf{M}_{d,e} \end{bmatrix},\ \mathbf{K}_d = \begin{bmatrix} \mathbf{K}_{d,b} & \mathbf{0}_{3\times6} \\ \mathbf{0}_{6\times3} & \mathbf{K}_{d,e} \end{bmatrix} \tag{48}$$

$$\mathbf{K}_p = \begin{bmatrix} \mathbf{K}_{p,b} & \mathbf{0}_{3\times6} \\ \mathbf{0}_{6\times3} & \mathbf{K}_{p,e} \end{bmatrix},\ \boldsymbol{F}_{des}^{*} = \begin{bmatrix} \mathbf{0}_{3\times1} \\ \boldsymbol{F}_{des} \end{bmatrix} \tag{49}$$

The closed-loop system error dynamics for the S/C attitude and the EE pose are given by,

$$\mathbf{M}_d\,\ddot{\mathbf{e}} + \mathbf{K}_d\dot{\mathbf{e}} + \mathbf{K}_p\,\mathbf{e} = -\boldsymbol{F}_{ext}^{*} + \boldsymbol{F}_{des}^{*} \tag{50}$$

Using (39) and considering a redundant number of RWs (i.e., $N_{rw} > 3$), the RWs and joints actuator inputs are,

$$\mathbf{Q}_c = \begin{bmatrix} \boldsymbol{\tau}_{rw}^{T} & \boldsymbol{\tau}^{T} \end{bmatrix}^{T} = (\bar{\mathbf{J}}_c^{*}\,\bar{\mathbf{J}}_c^{T^{*}})^{-1}\,\bar{\mathbf{J}}_c^{*}\,\mathbf{Q}_{contr} \tag{51}$$

The subset error dynamics for the S/C attitude are,

$$\ddot{\mathbf{e}}_b + \mathbf{K}_{d,b}\dot{\mathbf{e}}_b + \mathbf{K}_{p,b}\mathbf{e}_b = \mathbf{0}_{3\times1} \tag{52}$$

The chaser's S/C orientation error transient response during both phases is defined by the selection of the damping coefficient ζ_b and the natural frequency $\omega_{n,b}$ characterizing a desired second order response. Therefore, the diagonal matrices $\mathbf{K}_{d,b}$ and $\mathbf{K}_{p,b}$ are defined by the desired ζ_b and $\omega_{n,b}$ as

$$\mathbf{K}_{d,b} = 2\,\zeta_b\,\omega_{n,b}\,\mathbf{I}_3 \tag{53}$$

$$\mathbf{K}_{p,b} = \omega_{n,b}^{2}\,\mathbf{I}_3 \tag{54}$$

The EE response must differ between the free-space and contact phases; therefore, the proposed controller is analyzed separately for each phase, next.

A. *Free – space* phase

In the *free-space phase*, the external force $\boldsymbol{F}_{ext}$ vanishes, and consequently the desired force $\boldsymbol{F}_{des}$, defined as a function of $\boldsymbol{F}_{ext}$, also becomes zero. Then, the EE trajectory following is achieved, since the CCC controller results in the following EE error dynamics,

$$\mathbf{M}_{d,e}^{f}\ddot{\mathbf{e}}_e^{f} + \mathbf{K}_{d,\mathrm{e}}^{f}\dot{\mathbf{e}}_e^{f} + \mathbf{K}_{p,\mathrm{e}}^{f}\mathbf{e}_e^{f} = \mathbf{0}_{6\times1} \tag{55}$$

where,

$$\mathbf{e}_e^{f} = \mathbf{x}_e - \mathbf{x}_{e,d}^{f} \tag{56}$$

The vector $\mathbf{x}_{e,d}^{f}$ is the desired EE pose in the free-space phase, given by,

$$\mathbf{x}_{e,d}^{f} = \mathbf{x}_e^{in} - \mathbf{S}(t)(\mathbf{x}_e^{fin} - \mathbf{x}_e^{in}) \tag{57}$$

where $\mathbf{x}_e^{in}$ is the initial pose of the chaser's EE in free-space phase, $\mathbf{x}_e^{fin}$ is the corresponding chaser's EE pose at the moment of contact, and $\mathbf{S}(t)$ is a 6x6 diagonal matrix with fifth-order polynomial elements, function of the path arc length parameterization $s(t)$, [10].

The chaser's EE pose error transient response in the free-space phase is defined by the selection of the damping ratio ζ_e^{f} and the natural frequency $\omega_{n,\mathrm{e}}^{f}$ characterizing a desired second order response. In the *free-space phase*, the CCC controller corresponds to a model-based PD control law. In this case, the diagonal matrices $\mathbf{M}_{d,\mathrm{e}}^{f}$, $\mathbf{K}_{d,\mathrm{e}}^{f}$ and $\mathbf{K}_{p,\mathrm{e}}^{f}$ are,

$$\mathbf{M}_{d,\mathrm{e}}^{f} = m_{d,\mathrm{e}}^{f}\,\mathbf{I}_6 \tag{58}$$

$$\mathbf{K}_{d,\mathrm{e}}^{f} = 2\,\zeta_e^{f}\,\omega_{n,\mathrm{e}}^{f}\,m_{d,\mathrm{e}}^{f}\,\mathbf{I}_6 \tag{59}$$

$$\mathbf{K}_{p,\mathrm{e}}^{f} = \omega_{n,\mathrm{e}}^{f2}\,m_{d,\mathrm{e}}^{f}\,\mathbf{I}_6 \tag{60}$$

where $m_{d,\mathrm{e}}^{f} > 0$ can be chosen arbitrarily.

B. *Contact* phase

In the *contact phase*, effective contact force regulation is achieved. The application of the controller results in the following EE error dynamics,

$$\mathbf{M}_{d,e}^{c}\ddot{\mathbf{e}}_e^{c} + \mathbf{K}_{d,\mathrm{e}}^{c}\dot{\mathbf{e}}_e^{c} + \mathbf{K}_{p,\mathrm{e}}^{c}\mathbf{e}_e^{c} = -\boldsymbol{F}_{ext} + \boldsymbol{F}_{des} \tag{61}$$

where $\mathbf{e}_e^{c}$ is the EE pose error at the contact phase,

$$\mathbf{e}_e^{c} = \mathbf{x}_e - \mathbf{x}_{e,d}^{c} \tag{62}$$

where $\mathbf{x}_{e,d}^{c}$ is the desired EE trajectory pose during the contact phase, given by,

$$\mathbf{x}_{e,d}^{c} = \mathbf{x}_t = \begin{bmatrix} \mathbf{r}_t^{T} & \boldsymbol{\theta}_t^{T} \end{bmatrix}^{T} \tag{63}$$

where $\mathbf{r}_t$ and $\boldsymbol{\theta}_t$ are the target position and the Euler angles vector, respectively.

Assuming point contact between the EE and the target, only forces are developed between them. If friction is negligible, then only normal to the surface forces are developed which can be approximated by a spring of stiffness k_e and damping b_e [10] - [11].

The tracking error $\mathbf{e}_e^c$ as defined by (62) - (63) is the position and orientation error between the EE and the target. The component of this error vector along the contact normal direction directly corresponds to the penetration depth δ_e between the two bodies, i.e.,

$$\delta_e = \mathbf{e}_e^c \cdot \mathbf{n} \tag{64}$$

where $\mathbf{n}$ is the normal unit vector.

Therefore, controlling the error $\mathbf{e}_e^c$ effectively means controlling the magnitude of the contact force $\boldsymbol{F}_{ext}$, as both variables are directly related via a spring-damper model, i.e.,

$$\boldsymbol{F}_{ext} = -k_e\, \mathbf{e}_e^c \cdot \mathbf{n} - b_e\, \dot{\mathbf{e}}_e^c \cdot \mathbf{n} \tag{65}$$

Note that the orientation error contained in $\mathbf{e}_e^c$ may also contribute to the penetration in curved contact geometries, but in this work, we focus on the translational component along the contact normal, which dominates the normal force response in point or planar contact models.

The desired force/ moment $\boldsymbol{F}_{des}$, introduced to obtain non-zero steady state force during contact, must be zero in the free-space phase ensuring zero tracking error, while during the contact phase it must be non-zero, to ensure the continuous contact, [10] - [11]. Therefore,

$$\boldsymbol{F}_{des} = f_d \frac{\|\boldsymbol{F}_{\mathbf{ext}}\|}{\|\boldsymbol{F}_{\mathbf{ext}}\| + a_2} \mathbf{n} \tag{66}$$

where the parameter a_2 is chosen small enough, and f_d sets the desired steady-state value of the contact force and $\|(\cdot)\|$ denotes the norm of vector $(\cdot)$.

To select the controller gains at the contact phase, the chaser EE pose error transient response in the contact phase is defined by the selection of the damping ratio ζ_e^c and the natural frequency $\omega_{n,\mathrm{e}}^c$ characterizing a desired second order response. Therefore, the controller gain matrices $\mathbf{M}_{d,\mathrm{e}}^c$, $\mathbf{K}_{d,\mathrm{e}}^c$ and $\mathbf{K}_{p,\mathrm{e}}^c$ are defined by the desired ζ_e^c and $\omega_{n,\mathrm{e}}^c$ as,

$$\mathbf{M}_{d,\mathrm{e}}^c = m_{d,\mathrm{e}}^c\, \mathbf{I}_6 \tag{67}$$

$$\mathbf{K}_{d,\mathrm{e}}^c = (2\zeta_e^c\, \omega_{n,\mathrm{e}}^c\, m_{d,\mathrm{e}}^c - b_e)\mathbf{I}_6 \tag{68}$$

$$\mathbf{K}_{p,\mathrm{e}}^c = (\omega_{n,\mathrm{e}}^{c2}\, m_{d,\mathrm{e}}^c - k_e)\mathbf{I}_6 \tag{69}$$

where k_e is the spring stiffness along the contact direction, b_e is the contact damping and the gain $m_{d,\mathrm{e}}^c$ is selected considering that its minimum value must be,

$$m_{d,\mathrm{e,min}}^c = \max\left(\frac{k_e}{\omega_{n,\mathrm{e}}^{c2}},\ \frac{b_e}{2\zeta_e^c\, \omega_{n,\mathrm{e}}^c}\right) \tag{70}$$

to guarantee system stability during the contact phase, i.e., positive defined gain matrices $\mathbf{M}_{d,\mathrm{e}}^c$, $\mathbf{K}_{d,\mathrm{e}}^c$, $\mathbf{K}_{p,\mathrm{e}}^c$.

The CCC achieves both trajectory tracking in the *free-space phase* and force regulation in the *contact phase* by appropriately selecting the control gains. Specifically,

- During *free-space* phase, the gains are chosen according to (53) - (54) and (58) - (60) to ensure S/C and EE trajectory tracking.
- During *contact phase*, the gains are reconfigured based on (53) - (54) and (66) - (70) to ensure accurate S/C trajectory tracking and modulate the contact force.

To avoid controller switching during the EE motion in two phases, one approach is to apply common gains (either those designed for the free-phase or for the contact-phase) on both phases, as proposed in [10] - [11]. However, in this case, it can be shown that the EE error response, defined by the damping ratio ζ_e^c and the natural frequency $\omega_{n,e}^c$ at the contact phase, depends on the EE error response at the free-space phase, defined by the damping ratio ζ_e^f and the natural frequency $\omega_{n.e}^f$, and vice versa, i.e., [10]

$$\zeta_e^c = \zeta_e^f \sqrt{\frac{k_{d,\mathrm{e}}}{k_{d,\mathrm{e}} + k_e}} \quad , \quad \omega_{n,e}^c = \omega_{n,e}^f \sqrt{\frac{k_{d,\mathrm{e}} + k_e}{k_{d,\mathrm{e}}}} \tag{71}$$

where $k_{d.\mathrm{e}} = k_{d.\mathrm{e}}^f = k_{d.\mathrm{e}}^c$, since common gains are chosen.

Therefore, during the contact phase, choosing the control gains for an overdamped response (i.e. $\zeta_e^c > 1$), a continuous impact could be achieved. However, since $\zeta_e^c < \zeta_e^f$, see (71), this choice would result in an overdamped response in the free-space, which is undesirable, as the error response will be sluggish and the EE may not be driven to the contact point with the proper desired conditions leading to large contact forces and contact loss in the contact phase. On the other hand, a selection of control gains for a critically damped or underdamped response in the free space will yield an underdamped response (i.e. $0 < \zeta_e^c < 1$) in the contact phase, resulting in undesired force response overshoots or even in loss of contact, [10]. Therefore, the controller gains are selected independently for each phase (free-space and contact) to satisfy the specific performance requirements of each phase, while ensuring a smooth transition between the two phases without the need for controller switching. This is achieved using the following nonlinear functions which depend on the existence or not of $\boldsymbol{F}_{ext}$:

$$\mathbf{M}_{d,e} = \mathbf{M}_{d,e}^f\, w_1\left(\|\boldsymbol{F}_{\mathbf{ext}}\|\right) + \mathbf{M}_{d,e}^c\, w_2\left(\|\boldsymbol{F}_{\mathbf{ext}}\|\right) \tag{72}$$

$$\mathbf{K}_{d,e} = \mathbf{K}_{d,e}^f w_1\left(\|\boldsymbol{F}_{\mathbf{ext}}\|\right) + \mathbf{K}_{d,e}^c w_2\left(\|\boldsymbol{F}_{\mathbf{ext}}\|\right) \tag{73}$$

$$\mathbf{K}_{p,e} = \mathbf{K}_{p,e}^f w_1\left(\|\boldsymbol{F}_{\mathbf{ext}}\|\right) + \mathbf{K}_{p,e}^c\, w_2\left(\|\boldsymbol{F}_{\mathbf{ext}}\|\right) \tag{74}$$

where

$$w_1\left(\|\boldsymbol{F}_{\mathbf{ext}}\|\right) = \frac{\left|1 - \|\boldsymbol{F}_{\mathbf{ext}}\|/a_1\right|}{1 + a_1\|\boldsymbol{F}_{\mathbf{ext}}\|} \quad , \quad w_2\left(\|\boldsymbol{F}_{\mathbf{ext}}\|\right) = \frac{\|\boldsymbol{F}_{\mathbf{ext}}\|}{\|\boldsymbol{F}_{\mathbf{ext}}\| + a_2} \tag{75}$$

where the parameters a_1 and a_2 are chosen large enough and small enough, respectively, so that $\mathbf{M}_{d,e} = \mathbf{M}_{d,e}^f$, $\mathbf{K}_{d,e} = \mathbf{K}_{d,e}^f$ and $\mathbf{K}_{p,e} = \mathbf{K}_{p,e}^f$ in free-space phase, i.e., when $\|\boldsymbol{F}_{\mathbf{ext}}\| = 0$, and $\mathbf{M}_{d,e} = \mathbf{M}_{d,e}^c$, $\mathbf{K}_{d,e} = \mathbf{K}_{d,e}^c$ and $\mathbf{K}_{p,e} = \mathbf{K}_{p,e}^c$ during the contact phase, i.e., when $\|\boldsymbol{F}_{\mathbf{ext}}\| \neq 0$.

The desired trajectory $\mathbf{x}_{e.d}$ in (40) is defined as,

$$\mathbf{x}_{e,d}(t) = \mathbf{x}_{e,d}^f(t)\, w_1\left(\|\boldsymbol{F}_{\mathbf{ext}}\|\right) + \mathbf{x}_{e,d}^c(t)\, w_2\left(\|\boldsymbol{F}_{\mathbf{ext}}\|\right) \tag{76}$$

so that $\mathbf{x}_{e,d}(t) = \mathbf{x}_{e,d}^f(t)$ in free-space phase and $\mathbf{x}_{e.d}(t) = \mathbf{x}_{e.d}^c(t)$ during the contact phase.

IV. Example

To validate the effectiveness of the proposed controller under realistic physical conditions, simulations are conducted in a high-fidelity environment using MATLAB/Simscape. This

choice ensures that contact interactions and system behavior are governed by an independent physics-based environment, thus providing a reliable verification of the proposed approach. A 3 DoF manipulator is employed, as shown in Fig. 2. The system parameters are presented in Table I. These parameters correspond to the planar Space Robotics Emulator (SRE) shown in Fig. 3.

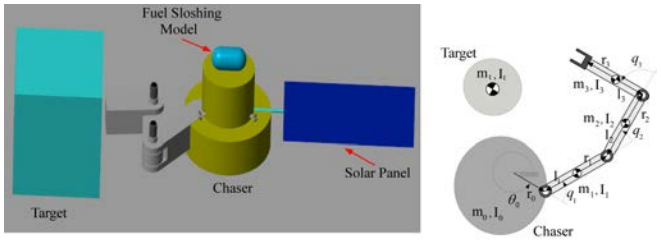

Fig. 2. (a) Simscape chaser and target models, (b) Parameters definition.

TABLE I. PARAMETERS OF THE CHASER SHOWN IN FIG. 2.

Body	m_i (kg)	r_i (m)	l_i (m)	I_i (kg m^2)
0	19.7	$[0\ 0.16]^T$	-	0.616
1	0.23	0.185	0.185	0.028
2	0.38	0.143	0.143	0.018
3	1.15	0.129	0.144	0.007

The target, of mass $m_t = 16.7kg$ and moment of inertia $I_t = 0.4\,kg\,m^2$, is initially at rest at $(x_t^{in}, y_t^{in}) = (0, 3.7)m$ with orientation $\theta_t^{in} = 0^0$. The chaser EE is driven from an initial position $(x_e^{in}, y_e^{in}) = (0.55, 3.21)m$ with orientation $\theta_e^{in} = 95^0$ to the target's position with final orientation $\theta_e^{fin} = 90^0$. The initial position of the S/C Center of Mass (CoM) and the S/C orientation are $(x_b^{in}, y_b^{in}) = (0, 0)m$ and $\theta_b^{in} = 0^0$, respectively. For the desired task, S/C attitude must remain constant.

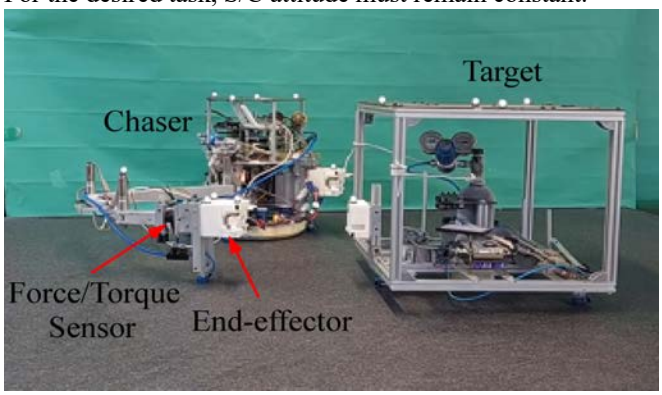

Fig. 3. The SRE at the National Technical University of Athens (NTUA).

Although the CCC is based on the system's rigid body dynamics, the system is subject to additional dynamic effects such as the flexible solar panels motion and fuel sloshing, which may introduce undesired disturbances. Here, these unmodeled dynamics are explicitly incorporated in MATLAB/Simscape Multibody environment. A solar panel is mounted on the S/C, with its properties listed in Table II.

The sloshing fuel is represented by a mass $m_s = 1kg$ connected via an equivalent spring-damper system of stiffness $k_s = 0.41\,Nm$, and damping coefficient $b_s = 0.02\,Nms$.

The contact interaction between the chaser and the target is modeled using the *Spatial Contact Force* block in Simscape, implemented as a linear spring with stiffness $k_e = 10^3\,kN/m$ and damping $b_e = 100\,Nms$. Solid geometries were selected to ensure smooth and physically consistent contact forces (point clouds were not used due to their tendency to produce less stable force profiles).

TABLE II. PROPERTIES OF THE S/C SOLAR PANEL.

Young's Modulus E (N/m^2)	*Density* ρ (kg/m^3)	*Length* L (m)	*Width* W (m)	*Height* H (m)
15*10^6	2700	0.75	0.002	0.3

Manipulator joint angles are measured via encoders, while position measurements for S/C, EE and target are given by a vision system (cameras). Contact forces are measured with a force/torque sensor on the manipulator wrist. Measurement noise is detailed in Table III.

TABLE III. NOISE CHARACTERISTICS

Measurement	*Sensor*	*Variance* (σ^2)
Joint angle	Encoder	$q^2/12$
Position (S/C, target, EE)	Cameras	0.000015^2
Contact Force	Force/ torque sensor	0.0077^2

The precision q of the encoder position depends on the encoder counts; for a 500 counts encoder, it is set equal to $q = 0.003\,\text{rad}$.

Assuming the use of first difference, the estimated variances of the joint rates σ_{qdot}^2 and the S/C, EE and target velocities σ_{xdot}^2 are, [12]

$$\sigma_{qdot}^2 = \frac{2}{\Delta T^2}\frac{q^2}{12}\ ,\ \sigma_{xdot}^2 = \frac{2}{\Delta T^2}0.000015^2 \tag{77}$$

where the sampling period is chosen as $\Delta T = 0.05\,\text{s}$.

The S/C angular velocity is obtained from an Inertial Measurement Unit (IMU). The IMU gyro measurements were simulated as proposed in [11] - [14]

$$\tilde{\boldsymbol{\omega}}_b = \boldsymbol{\omega}_b + \mathbf{b}_\omega + \mathbf{n}_\omega \quad ,\quad \dot{\mathbf{b}}_\omega = \mathbf{n}_{b\omega} \tag{78}$$

where $\boldsymbol{\omega}_b$ is the true angular velocity and $\tilde{\boldsymbol{\omega}}_b$ is the corresponding measurement of the angular velocity. The term $\mathbf{b}_\omega$ is the gyroscope bias, while the terms $\mathbf{n}_\omega$ and $\mathbf{n}_{b\omega}$ represent white Gaussian noise with initial bias $\mathrm{b}_{\omega,0} = 0.1\,\text{deg/hr}$, zero mean and standard deviations $\sigma_\omega = 3.1623\cdot10^{-4}\,\mu\text{rad/s}^{3/2}$, $\sigma_{b\omega} = 0.31623\,\mu\text{rad/s}^{1/2}$, [11].

Moreover, due to the different control rates—10 Hz for the S/C and 1000 Hz for the manipulator—in this work, multi-rate effects have been considered in controller design to maintain stability under GNC constraints, [15].

During on-orbit operations, both the S/C mass and inertia vary due to fuel consumption. Consequently, the position of the S/C CoM also shifts over time. To evaluate the robustness of the proposed controller, these parameters must be treated as system uncertainties. Furthermore, the contact between the EE and the target is modeled as a spring-damper system with nominal stiffness k_e and damping coefficient b_e. In practice,

this model is a simplification, and at minimum, parametric uncertainty in these contact dynamics should be considered to ensure a realistic robustness analysis of the controller. In this study, a ±10% uncertainty is assumed for all these parameters.

In this example, the effectiveness of the CCC is first evaluated against a baseline model-based PD controller and a classical impedance controller, under the assumption of ideal conditions, i.e., no flexible appendages, no uncertainties, noiseless measurements, no multi-rate effects. In this case, the system's controllable vector is given by,

$$\mathbf{v}_{cont} = [\dot{\theta}_b \quad \dot{x}_e \quad \dot{y}_e \quad \dot{\theta}_e]^T \tag{79}$$

where $\dot{\theta}_b$ is the S/C angular velocity and $\dot{\mathbf{r}}_e = [\dot{x}_e \quad \dot{y}_e]^T$, $\dot{\theta}_e$ are the EE linear and angular velocities, respectively.

The applied actuation vector is,

$$\mathbf{Q}_c = \begin{bmatrix} \tau_{rw} & \boldsymbol{\tau}^T \end{bmatrix}^T \tag{80}$$

where $\boldsymbol{\tau} = [\tau_1 \quad \tau_2 \quad \tau_3]^T$ is the column vector of the manipulator joint torques and τ_{rw} is the RW torque.

The following control laws are studied and compared considering the resulting contact forces.

(a) Model – based PD (MBPD) control law

The MBPD control law is given by,

$$\mathbf{Q}_{contr} = \bar{\mathbf{M}}^* \mathbf{u} + \bar{\mathbf{c}}^* \tag{81}$$

where

$$\mathbf{u} = \begin{bmatrix} \mathbf{u}_b^T & \mathbf{u}_e^T \end{bmatrix}^T = \ddot{\mathbf{z}}_d - \mathbf{K}_d (\dot{\mathbf{z}} - \dot{\mathbf{z}}_d) - \mathbf{K}_p (\mathbf{z} - \mathbf{z}_d) \tag{82}$$

where $\mathbf{z}$ is defined in (46) and the controller gains are defined as

$$\mathbf{K}_d = 2\zeta\, \omega_n\, \mathbf{I}_4 \tag{83}$$

$$\mathbf{K}_p = \omega_n^2\, \mathbf{I}_4 \tag{84}$$

The controller gains are selected to achieve desired critically damping responses (i.e., $\zeta = 1$) in free-space phase with $\omega_n = 0.6\, rad/s$ (i.e., settling time $t_s = 10\, s$) for the controllable variables defined in (79). The desired trajectories for these variables are given by (57). The force response is shown in Fig. 4(a).

(b) Classical impedance control law

The classical impedance control law is given by,

$$\mathbf{Q}_{contr} = \bar{\mathbf{M}}^* \mathbf{u} + \bar{\mathbf{c}}^* - \bar{\mathbf{J}}_e^{T^*} \boldsymbol{F}_{ext} \tag{85}$$

where

$$\mathbf{u} = \ddot{z}_d + \mathbf{M}_d^{-1} [-\mathbf{K}_d (\dot{\mathbf{z}} - \dot{\mathbf{z}}_d) - \mathbf{K}_p (\mathbf{z} - \mathbf{z}_d) - \boldsymbol{F}_{ext}^*] \tag{86}$$

where $\mathbf{z}$ is defined in (46) and the controller gains are defined as,

$$\mathbf{M}_d = m_d\, \mathbf{I}_4 \tag{87}$$

$$\mathbf{K}_d = (2\zeta\, \omega_n\, m_d - b_e)\, \mathbf{I}_4 \tag{88}$$

$$\mathbf{K}_p = (\omega_n^2\, m_d - k_e)\, \mathbf{I}_4 \tag{89}$$

the gain m_d is selected as,

$$m_d = 2 \max\left(\frac{k_e}{\omega_n^2},\ \frac{b_e}{2\zeta\, \omega_n}\right) \tag{90}$$

The controller gains are selected to achieve desired a critically damping response in contact phase with $\omega_n = 7.5\, rad/s$ (i.e., settling time $t_s = 0.8\, s$ during contact) for the controllable variables defined in (79). The desired trajectories are given by (57). In this case, the resulting response of the contact force is shown in Fig. 4(b).

Although the impedance controller demonstrates improved contact force response compared to the model-based PD controller, its performance is still unsatisfactory, even under ideal operating conditions, suggesting the need for more advanced control strategies.

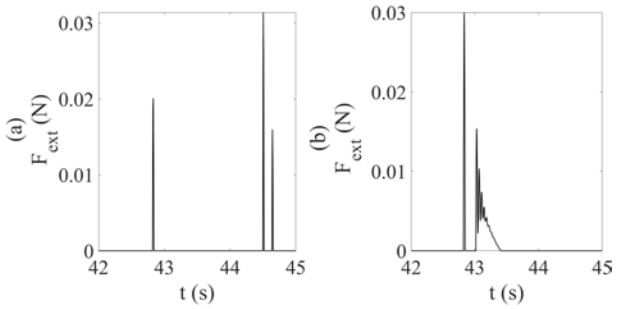

Fig. 4. Force response: (a) Model-based PD control (b) Classical impedance control.

(c) Coordinated Compliant Control (CCC) law

To achieve precise contact force regulation, the proposed CCC controller, given by (38) and (44), is applied. Again, the S/C control in both phases is achieved by selecting the gains by (53) - (54) with $\zeta_b = 1$, $\omega_{n,b} = 0.6\, rad/s$. In *free-space phase*, EE trajectory tracking is ensured by selecting the controller gains according to (58) - (60) with $\zeta_e^f = 1$, $\omega_{n,e}^f = 0.6\, rad/s$. During *contact phase*, force regulation is achieved by tuning the gains based on (66) - (70), with $\zeta_e^c = 1$, $\omega_{n,e}^c = 7.5\, rad/s$, setting also $m_{d,e}^c = 2\, m_{d,\mathrm{e,min}}^c$ and a desired steady-state contact force of $f_d = 1N$. The avoid controller switching, the control gains are given by (72) - (74) and the desired trajectory is given by (76) with $a_1 = 10^{12}, a_2 = 10^{-12}$. The force response is shown in Fig. 5(a). It can be observed that, under ideal operating conditions, the contact force converges smoothly to the desired value, confirming that the system achieves the intended behavior.

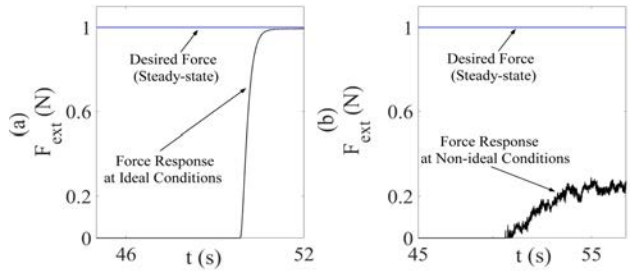

Fig. 5. Force response (CCC): (a) Ideal operating conditions and (b) non-ideal operating conditions.

Subsequently, the feasibility of deploying the proposed approach in *non-ideal* operating conditions, i.e., the presence of flexibilities, model uncertainties, multi-rate effects (i.e., 10 Hz for the S/C and 1000 Hz for the manipulator) and measurement noise, as described earlier, is demonstrated. Under these operating conditions, the contact force response

is illustrated in Fig. 5(b). As expected, the response deviates from the ideal behavior observed previously (Fig. 5(a)). However, the contact force remains consistently non-zero, indicating that physical contact between the EE and the target is maintained throughout the interaction. This is a desirable outcome, as the primary control objective during contact is not the precise tracking of the force reference, but rather the preservation of contact for a sufficiently long duration to allow successful task execution. The S/C attitude and EE pose error responses are shown in Fig. 6 and the required RW and joint torques are presented in Fig. 7. Snapshots of the resulting capture task are shown in Fig. 8.

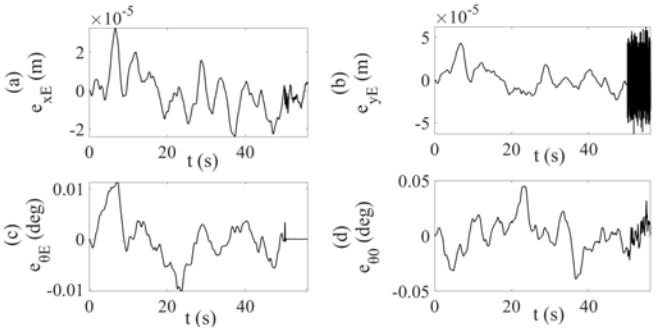

Fig. 6. Error response: (a) – (c) chaser EE pose, (d) chaser S/C attitude.

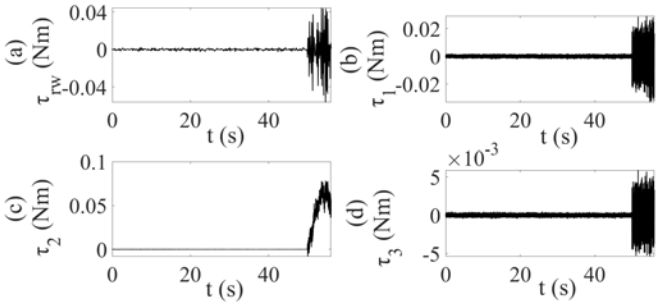

Fig. 7. (a) RW torque and (b) – (d) Manipulator joint torques.

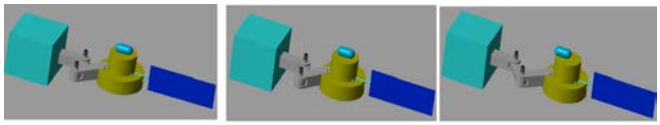

Fig. 8. Chaser motion snapshots: (a) Initial chaser position, (b) Free-phase motion and (c) Contact phase motion.

V. Conclusion

A Coordinated Compliant Control (CCC) law for SMS aimed at enabling safe and robust target capture in on-orbit servicing and assembly missions has been developed. The proposed controller ensured accurate trajectory tracking in free-space motion and safe force regulation during physical contact, while enabling a smooth transition between the two phases without the need for controller switching. Additionally, the proposed controller guaranteed attitude preservation of the chaser spacecraft, addressing critical safety concerns such as communication stability and power alignment. Although the controller explicitly accounts only for SMS rigid-body dynamics, it was shown that it demonstrates strong robustness under various realistic non-ideal conditions, including flexible appendage vibrations, fuel sloshing, multi-rate effects and sensor noise. Simulation results confirmed the effectiveness and resilience of the approach. Future work will focus on experimental validation using the SRE.

References

[1] Papadopoulos, E., Aghili, F., Ma, O., and Lampariello, R. "Robotic Manipulation and Capture in Space: A Survey," *Frontiers: Robotics & AI - Space Robotics*, 9, July 2021.

[2] Nair, M. H. Rai, M. C., Poozhiyil M., Eckersley, S., Kay, S., and Estremera, J., "Robotic Technologies for In-Orbit Assembly of a Large Aperture Space Telescope: A Review," *Advances in Space Research*, Vol. 74 (10), November 2024, pp. 5118-5141.

[3] Palma, P., Seweryn, K., & Rybus, T., "Impedance Control Using Selected Compliant Prismatic Joint in a Free-Floating Space Manipulator," *Aerospace*, 9 (8), 2022, p. 406.

[4] Liu, D., & Chen, L., "Dual-Arm Space Robot On-Orbit Operation of Auxiliary Docking Prescribed Performance Impedance Control," *Aerospace*, 11 (11), 2024, p. 867.

[5] Xi, H., Chen, B., Zhang, R., Zhang, X., and Luo, M., "Adaptive optimal concurrent control for detumbling space non-cooperative target via multipoint repeated contact," *Aerospace Science and Technology*, Vol. 154, 2024, p. 109473.

[6] Stolfi, A., Gasbarri, P., and Sabatini, M., "A Parametric Analysis of a Controlled Deployable Space Manipulator for Capturing a Non-Cooperative Flexible Satellite," *Acta Astronautica*, Vol. 148, 2018, pp. 317 – 326.

[7] Liu, X., Wang, R., Cai, G., and Lin, Z., "Resistance Control: A New Collision Control Method for On-orbit Service," *Nonlinear Dynamics*, Vol. 111, 2023, pp. 13969 – 13984.

[8] Tao, D., Zhang, Q., Chu, X., Zhou, X., and Zhao, L., "Impedance-Sliding Mode Control with Force Constraints for Space Robots Capturing Non-Cooperative Objects," *IEEE Access*, Vol. 9, 2021, pp. 160163–160174.

[9] Wang, R., Liu, X., Ji, R., Cai, G., and Xu, F.., "Compliance Resistance Collision Control for Operating a Space Robot to Capture a Non-Cooperative Spacecraft," *Aerospace Science and Technology*, Vol. 153, 2024, p. 109425.

[10] Nanos, K., Xydi-Chrysafi, F., and Papadopoulos, E., "On Impact Deorbiting for Satellites Using a Prescribed Impedance Behavior," *IEEE 58th Conference on Decision and Control,* Nice, France, Dec. 11-13, 2019, pp. 2126 – 2131.

[11] Nanos, K., and Papadopoulos, E., "On the Design of Coordinated Impedance Control Laws for De-orbiting and De-Spinning of Cooperative Satellites," *30th IEEE Mediterranean Conference on Control and Automation*, (MED '22), Vouliagmeni, Greece, June 28-July 1, 2022, pp. 577 - 582.

[12] Armstrong, B., "On Finding Exciting Trajectories for Identification Experiments Involving Systems with Nonlinear Dynamics," *International J. of Robotics Research*, v. 8, n. 6, December 1989, pp. 28-48.

[13] Crassidis, J.L., and Markley, L.F., "Unscented Filtering for Spacecraft Attitude Estimation," *Journal of Guidance, Control and Dynamics*, Vol. 26, No. 4, August 2003, pp. 536-542.

[14] Nanos, K., and Papadopoulos, E., "On Parameter Estimation of Space Manipulator Systems with Flexible Joints Using the Energy Balance," *IEEE International Conference on Robotics and Automation (ICRA '19)*, Montreal, Canada, May 20-24, 2019, pp. 3570-3576.

[15] De Stefano, M., Mishra, H., Balachandran, R., Lampariello, R., Ott. C., Secchi, C., "Multi-Rate Tracking Control for a Space Robot on a Controlled Satellite: A Passivity-Based Strategy," *IEEE Robotics and Automation Letters*, Vol. 4, No. 2, April 2019, pp. 1319 – 1326.

Acknowledgment

This work was partially funded by the European Union under Horizon Europe (grant No. 101136568 - HERON).